Available online at www.sciencedirect.com
ScienceDirect
Chemical Physics 328 (2006) 190–196
Chemical Physics
www.elsevier.com/locate/chemphys

A model two-dimensional potential for internal rotation of 9-methylanthracene studied by electronic spectroscopy and DFT calculations

Masayuki Nakagaki, Eriko Nishi, Kenji Sakota, Haruyuki Nakano, Hiroshi Sekiya *

Graduate School of Molecular Sciences, and Department of Chemistry, Faculty of Sciences, Kyushu University, 6-10-1 Hakozaki, Higashi-ku, Fukuoka 812-8581, Japan

Received 12 April 2006; accepted 28 June 2006
Available online 18 July 2006

Abstract

The S_1-S_0 fluorescence excitation and dispersed fluorescence spectra of 9-methylanthracene are measured in a supersonic free jet expansion. Several low-frequency bands assigned to the transitions between the internal rotational levels of the methyl group can not be fitted to the calculated energy levels obtained by the one-dimensional rotor model. We have introduced a two-dimensional model incorporating the coupling of the methyl rotation and an out-of-plane bending motion of the anthracene ring. The calculations based on this model reproduce the intensity distributions in the fluorescence excitation and dispersed fluorescence spectra as well as the frequencies of the internal rotational levels in the S_0 and S_1 state.

Keywords: Electronic spectrum; 9-Methylanthracene; Methyl group; Methyl rotation; Torsional potential; Supersonic jet; Steric repulsion; Excitation spectrum; Fluorescence; Two-dimensional model

1. Introduction

The analysis of the internal rotational potentials of the methyl group in the aromatic molecules provides information on non-covalent interaction, reorganization of electrons, and the intramolecular vibrational energy redistribution. In several methyl-substituted aromatic molecules, the internal rotational potentials of the methyl group in the S_0 and S_1 states were well reproduced with the one-dimensional model along the rotational angle of the methyl group [1–5]. The substitution of a methyl group generates three isomers, 1-, 2-, and 9-methylanthracene. The internal rotational potential of the methyl group in the three molecules strongly depends on the substituted position. In the previous study, we observed the fluorescence excitation (FE) and dispersed fluorescence (DF) spectra of 2- and 1-methylanthracence [6]. The internal rotational levels of the methyl group in the S_0 and S_1 states of 2-methylanthracene were well reproduced with the one-dimensional free rotor model. The relative intensities of the internal rotational levels of 2-methylanthracene were explained by the difference in the phase, which is the difference in the methyl rotational angles corresponding to the two potential minima or maxima in the S_0 and S_1 states. On the other hand, a prominent electronic origin was observed only in the FE and DF spectra of 1-methylanthracene since the phase of the methyl rotational potential does not change upon photoexcitation [6]. The one-dimensional free rotor model indicated that the phase of the potential of the methyl group in 1-methylanthacene does not change upon photo-excitation. For this reason only a prominent electronic origin was observed in the FE and DF spectra of 1-methylanthracene. Thus, the internal rotational potentials of the 2- and 1-methylanthra-

* Corresponding author. Tel./fax: +81 92 642 2574.
E-mail address: hsekiscc@mbox.nc.kyushu-u.ac.jp (H. Sekiya).

0301-0104/$ - see front matter © 2006 Elsevier B.V. All rights reserved.
doi:10.1016/j.chemphys.2006.06.043

cene can be described with the one-dimensional free rotor model due to minor interaction of the methyl group with the neighboring C–H hydrogen atoms in the two molecules. We demonstrated that the σ–π or σ–π* hyperconjugation effect introduced by Nakai and co-worker [7–11] can apply to elucidate the internal rotational barriers in the S_0 and S_1 states of 2- and 1-methylanthracene.

We observed the electronic spectra of 9-methylanthracene (9MA) as well as those of 2-, and 1-methylanthracene. Several vibronic bands are well resolved in the low-frequency region of the FE spectrum. The corresponding low-frequency bands are observed in the DF spectra. Some low-frequency bands are assigned to the internal rotation of the methyl group. However, the one-dimensional rotor model could not reproduce the observed levels. The internal rotation of the methyl group of 9MA may be described with sixfold potential such as the one of toluene. The barrier heights of sixfold rotational potentials for toluene and substituted toluene are very low (5–44 cm^{-1}) [1–4]. The effect of the steric repulsion on the methyl rotation must be much lager in 9MA than in 1MA, because the distance between the C–H hydrogen atom at the 1- or 8-position and the methyl hydrogen atoms of 9MA is significantly shorter than that between the C–H hydrogen at the 2-position and the methyl hydrogen atoms of 1MA. Therefore, the internal rotational levels of 9MA may be strongly perturbed due the steric repulsion. A similar interaction may occur in other methyl-substituted large aromatic molecules. However, the effect of the steric repulsion on the internal rotational potential in the methyl-substituted aromatic molecules has not been fully understood.

Syage et al. reported the electronic spectra of 9MA [12]. They considered that several low-frequency bands due to the rotation of the methyl group were involved, because such low-frequency vibrations were absent in anthracene [13]. However, no definite assignment was made. Very recently, Mordziński et al. also reported the electronic spectra of 9MA and 9-cyano-10-methylanthracence to investigate the internal rotation of the methyl group and the coupling of the motions of the two methyl groups [14]. They observed six low-frequency bands in the FE spectrum of 9MA. It was suggested that these bands could be reproduced with a one-dimensional model with potential parameters $V_6 = 70.4\ cm^{-1}$ and $V_4 = 19.1\ cm^{-1}$ in the S_0 and S_1 state, respectively, where V_6 and V_4 are the barrier heights of the sixfold and fourfold potentials. The result of Mordziński et al. on 9MA is not consistent with our preliminary analysis of the internal rotational potential of the methyl group, which will be described in this paper.

In the present work, we have analyzed the internal rotational potential of 9MA to investigate the interaction of the methyl group and the anthracene ring by introducing a two-dimensional model that incorporates a coupling of the methyl rotation and an out-of-plane bending motion of the anthracene ring. A characteristic feature of this interaction is discussed.

2. Experiment

9MA was purchased from Wako Pure Chemical Ind. Ltd., and was used without further purification. The experimental apparatus for the measurement of the FE and dispersed fluorescence (DF) spectra was essentially the same as that reported previously [15,16]. Briefly, 9MA was vaporized by heating the solid sample in a nozzle housing to 100–120 °C. Gas mixture of the vaporized molecules and helium was expanded into a vacuum chamber with a pulsed nozzle (General Valve Series 9, 0.5 mm orifice diameter). The backing pressure was 200–300 kPa. An excimer laser pumped dye laser system (Lumonics EX-600 and HD-300) excited the molecules seeded in the helium gas. FE spectrum was measured by monitoring total fluorescence with a photomultiplier tube (Hamamatsu 1P28A). DF spectra were measured with a monochromator equipped with a photomultiplier tube (Hamamatsu R955). The signal from the photomultiplier was fed into a digital oscilloscope (LeCroy 9310A) and processed by a PC.

3. Results and discussion

3.1. FE and DF spectra

Fig. 1 shows the $S_1 \leftarrow S_0$ FE spectrum of 9MA around the electronic origin region. The origin band is observed at 26933 cm^{-1}. Several bands are detected in the region $\Delta v = 0$–200 cm^{-1}. The FE spectrum in Fig. 1 is in agreement with the spectrum of Mordziński et al. [14]. The intensity distribution in this spectrum suggests the change of significant conformation by the $S_1 \leftarrow S_0$ excitation. Such low-frequency vibrations have not been reported in the FE spectrum of anthracene [13], therefore, the vibronic bands are ascribed to the transitions between the internal rotational levels arising from methyl rotation.

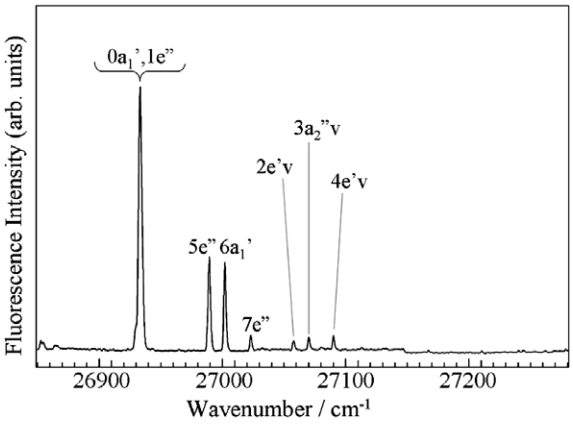

Fig. 1. FE spectrum of jet-cooled 9MA. The spectrum was obtained under the condition where the 0–0 transition was saturated to observe weak transitions. The assignment of vibronic states in S_1 was made by a two-dimensional model (see the text).

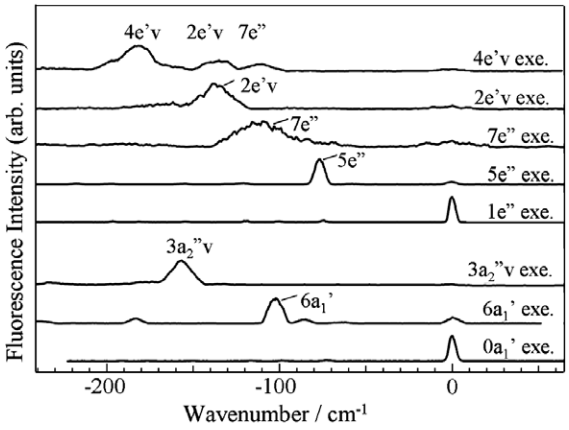

Fig. 2. DF spectra of jet-cooled 9MA. The assignment of vibrations in S_0 was made by a two-dimensional model (see the text).

Fig. 2 shows the DF spectra measured by exciting in each band of the FE spectrum. The vibrational distribution significantly depends on the upper state, and the strongest band in each DF spectrum may correspond to the same mode in S_1. The assignment for the internal rotational levels has been made by introducing a two-dimensional model, which is described in detail in Section 3.4.

3.2. Breakdown of one-dimensional model

In several aromatic molecules with a methyl group, the internal rotation of methyl group is analyzed with a one-dimensional rotor model [1–4,17]. The internal rotational Hamiltonian is expressed by

$$H(\theta) = -B\frac{d^2}{d\theta^2} + \frac{1}{2}\sum_n V_n(1-\cos n\theta) \quad (1)$$

where θ is the rotational angle between the one of the C–H bonds of the methyl group and the plane of the anthracene ring (Fig. 3), while B is the internal rotational constant. The Schrödinger equation is given by

$$H(\theta)\psi_m(\theta) = E_m\psi_m(\theta) \quad (2)$$

A set of free rotor basis functions $\cos(m\theta)$ and $\sin(m\theta)$ is employed to determine the eigenvalues of this Hamiltonian. The assignments for the rotational levels are made with a combination of the rotational quantum number $m(0,1,2,\ldots)$ and the symmetry species $\sigma(a_1', a_2', e', a_1'', a_2'', e'')$ of molecular symmetry group G_{12}. We attempted to reproduce the internal rotational levels observed in the LIF and DF spectra by using a model Hamiltonian in Eq. (1) where sixfold symmetry $V_6(\cos 6\theta)$ was assumed. We show an example of the calculated internal rotational levels with $B = 5.2\ \mathrm{cm}^{-1}$, $V_6 = 11\ \mathrm{cm}^{-1}$ in Fig. 4. The calculated energies are substantially deviated from the observed ones. In addition, some S_1-S_0 transitions are forbidden. Any values for B and V_6 could not reproduce the intensities of observed transitions from the $0a_1$' or 1e" levels in the S_0 state, even if the additional term (V_3) was added.

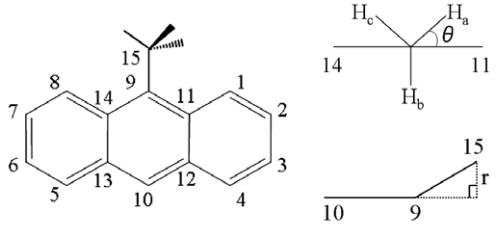

Fig. 3. Structure of 9MA and definition of parameters θ and r.

In order to examine the reason for the breakdown of the one-dimensional free rotor model we have calculated the normal modes of 9MA. All calculations were performed with a $G_{AUSSIAN}$ 03 program package [18]. Geometry optimization and the normal mode analysis were carried out for the optimized structures for the S_0 and S_1 states at the B3LYP/6-31+G(d,p) and CIS/6-31+G(d,p) levels, respectively. Two lowest frequency normal modes in the S_0 and S_1 state are drawn in Fig. 5, while the force constants and the reduced masses of these modes are listed in Table 1. In the S_0 state, both of the coordinates of the $\nu_{S0,1}$ and $\nu_{S0,2}$ modes are composed of the methyl rotation and an out-of-plane bending motion. The bending motion mainly consists of methyl wagging, where the methyl carbon atom deviates from the molecular plane of the anthracene ring, while the anthracene frame deviates from the plane due to the motion of the methyl carbon atom. In the optimized structure for the S_1 state, the methyl rotation and an out-of-plane bending motion are separated into two normal modes as illustrated in Fig. 5. The calculations suggest that the coupling between the methyl rotation and the out-of-plane bending vibration varies depending on the rotational angle θ. For example, at $\theta = 0°$ in the S_1 state, the two lowest modes are described as the combination

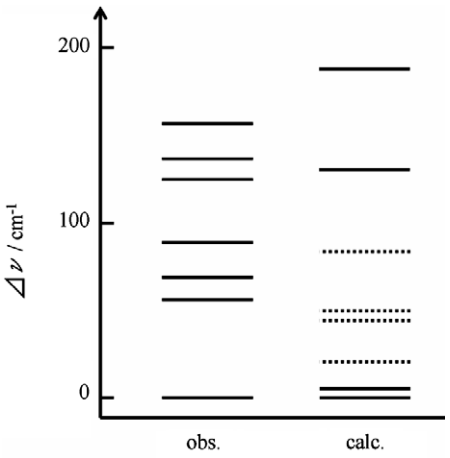

Fig. 4. Calculated internal rotational levels in S_1 of 9MA are compared with the observed ones. The calculated internal rotational levels were obtained by the one-dimensional free rotor model with $B = 5.2\ \mathrm{cm}^{-1}$ and $V_6 = 11\ \mathrm{cm}^{-1}$. The dotted lines indicate optically forbidden states in the V_6 potential.

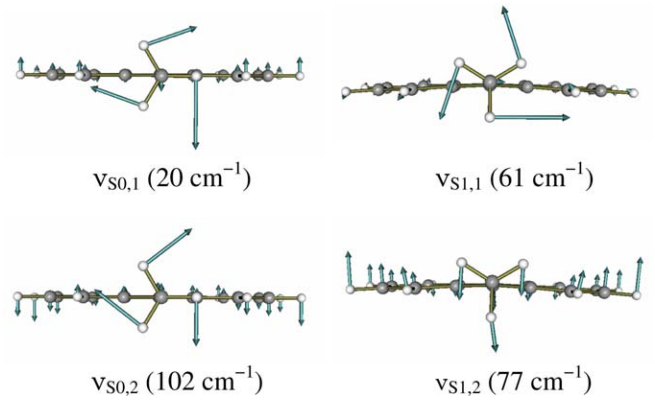

Fig. 5. Illustration of modes $\nu_{S0,1}$, $\nu_{S0,2}$, $\nu_{S1,1}$, and $\nu_{S1,2}$.

Table 1
Normal modes of 9MA in S_0 and S_1

Mode	ν/cm^{-1}	k/Nm^{-1}	μ/amu
$\nu_{S0,1}$	20	0.03	1.4368
$\nu_{S0,2}$	102	1.30	2.1316
$\nu_{S1,1}$	61	0.25	1.1272
$\nu_{S1,2}$	77	1.46	4.2266

of the methyl rotation and the out-of-bending motion, although one of them has an imaginary frequency.

3.3. Coupling of methyl rotation with out-of-plane bending motion

The rotational angle θ is 0° in the stable conformation of the S_0 state, where one of the C–H bonds of the methyl group lies in the plane of the anthracene ring (Fig. 3). The rotational angle was varied from 0° to 120° at 10° intervals. Single point energy calculations were carried out for the S_1 state by TD-DFT calculations at the B3LYP/6-31+G(d,p) level, where we used the optimized structures in the S_0 state. The potential energy curves for the methyl rotation thus obtained are shown in Fig. 6. The barrier heights of rotational potential for the S_0 and S_1 states of 9MA are 19 cm^{-1} and 11 cm^{-1}, respectively. These values are much smaller than the corresponding values for 2MA ($V_3 = 302$ and 215 cm^{-1} for S_0 and S_1) and 1MA ($V_3 = 790$ and 477 cm^{-1} for S_0 and S_1) [6]. The potential energy curve for the S_1 state has a minimum at $\theta = 0°$ as is the case of the S_0 state. However, the structure optimized for the S_1 state by CIS calculation has the rotational angle $\theta = 30°$. The difference in the stable angle θ arises from the employment of the structure optimized for the S_0 state to obtain the stable structure in the S_1 state. The anthracene ring of 9MA is planar at $\theta = 0°$, but it deviates from the planar structure due to rotation of the methyl group. The deviation from the planar structure is larger in the S_1 state than in the S_0 state. Therefore, the single point calculations using the S_0 state structures overestimate the potential energy in the S_1 state at $\theta = 30°$, and generates a phase difference in the internal rotational potential for the S_1 state when we apply the one-dimensional model.

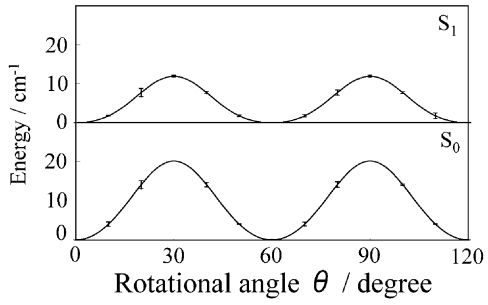

Fig. 6. Calculated potential energy curves for the S_0 and S_1 states as a function of the rotational angle θ.

In order to investigate the interaction between the methyl rotation and the out-of-plane vibration, we introduce a two-dimensional potential. The potential of the methyl rotation coupled with the motions of the out-of-plane bending mode should be described by using at least more than three coordinates. However, the calculations of the potential with the coordinates larger than three are not easy for this system. Therefore, we have introduced a parameter r, which is the distance between the carbon atom of the methyl group and the plane containing the center aromatic ring of anthracene expressed with a dummy atom (Fig. 3). The parameter r explicitly describes an out-of-plane bending motion of the methyl group, while the butterfly motion of the anthracene ring is implicitly involved in r. The sign of r is defined as the direction of displacement of the methyl carbon atom. The optimizations with two fixed parameters for the S_0 state and single point calculations for the S_1 state were carried out with DFT and TD-DFT methods at the B3LTP/6-31G level, respectively. The rotational angle θ was varied from 0° to 30° at 10° intervals, and the r value varied 0.14 Å to −0.14 Å at 0.02 Å intervals. To confirm the symmetry of potential energy surfaces, the calculations were carried out for the additional points with $\theta = 60°$, 90°, 120° and $r = 0.1$ Å, 0 Å, −0.1 Å.

Fig. 7 shows two-dimensional potential energy surfaces $V(\theta, r)$ along the coordinates of the methyl rotation and the out-of-plane motion of the methyl group. For the S_1 state, the most stable point is located at $\theta = 30°$. Best fit potential parameters are $V_6 = 14$ cm^{-1}, $k = 7387$ cm^{-1} Å^{-2}, and $K_{\theta r} = -250$ cm^{-1} Å^{-1} for the S_0 state, and $V_6 = 16$ cm^{-1}, $k = 4915$ cm^{-1} Å^{-2}, and $K_{\theta r} = -483$ cm^{-1} Å^{-1} for the S_1 state. These potential energy surfaces indicate that the methyl rotation couples with the out-of-plane bending motion, and the coupling is stronger in the S_1 state than in the S_0 state.

3.4. Two-dimensional model

On the basis of the potential energy surface in Fig. 7 we have introduced a two-dimensional model, in which the methyl rotation is coupled with an out-of-plane mode.

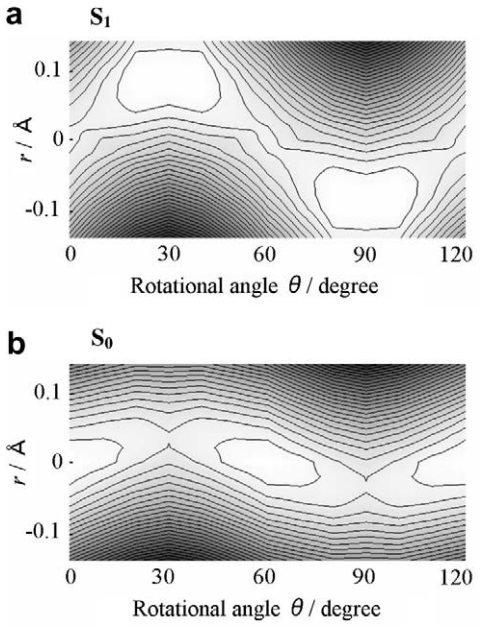

Fig. 7. Contour plots of potential energy surfaces $V(\theta,r)$ for S_1 (a) and S_0 (b). The light area is energetically higher than the gray area. The step between the isoenergetic contour is 5 cm^{-1}.

The out-of-plane bending mode has a_2'' symmetry and belongs to the G_{12} group. The two-dimensional model Hamiltonian is written as

$$H(\theta,q) = -B\frac{\partial^2}{\partial\theta^2} - \frac{\hbar^2}{2\mu}\frac{\partial^2}{\partial q^2} + \frac{1}{2}V_6'(1-\cos 6\theta) + \frac{1}{2}kq^2 + K_{\theta q}q\sin 3\theta \quad (3)$$

where q is the coordinate of the out-of-plane bending motion, and μ and k are the reduced mass and the force constant of q, and $K_{\theta q}$ is a coupling constant. The relation between V_6' in Eq. (3) and V_6 in Eq. (1) is derived from $\frac{\partial H}{\partial q} = 0$.

Table 2
Observed and calculated internal rotational levels in S_1 of 9MA[a]

$\Delta\nu/cm^{-1}$				Assignment
Observed[b]	Calculated[c]	Observed (Ref. [12])	Observed (Ref. [14])	
0	0	0	0	$1e''$
1	1			$0a_1'$
56	48	56	56	$5e''$
69	69	69	69	$6a_1'$
89	92	90	90	$7e'$
125	127	125	124	$2e'v$
137	132	137	136	$3a_2''v$
157	159	157	157	$4e'v$

[a] a_1' levels were excited from $0a_1'$ in S_0, and e'' levels were excited from $1e''$ in S_0.
[b] The accuracy of the frequencies are ± 1 cm^{-1}.
[c] Obtained with parameters $B = 2.1$ cm^{-1}, $V_6 = 20$ cm^{-1}, $k = 1.67$ Nm^{-1}, $K_{\theta q} = -5.16\times10^{-11}$ N, and $\mu = 2.13$ amu.

$$V_6 = V_6' - \frac{K_{\theta q}^2}{2k} \quad (4)$$

The kinetic coupling is neglected. The Schrödinger equation is given by

$$H(\theta,q)\psi(\theta,q) = E\psi(\theta,q) \quad (5)$$

$$\psi(\theta,q) = \sum_{m,v} C_{m,v}\psi_{\mathrm{m}}(\theta)\psi_{\mathrm{v}}(q) \quad (6)$$

Basis functions used are free rotor wave functions and harmonic oscillator wave functions, which involve the coordinates θ and q, respectively. The Hamiltonian matrix elements are written as

$$\langle m'_{\cos}, v'|H|m_{\cos}, v\rangle = \left[\left\{\left(m_{\cos}^2 B + \frac{V_6}{2}\right) + \frac{1}{200\pi c}\left(v+\frac{1}{2}\right)\left(\frac{k}{\mu}\right)^{\frac{1}{2}}\right\}\delta_{\mathrm{m,m'}} - \frac{V_6}{2}\left(\delta_{\mathrm{m+m',6+\delta_{|m-m'|,6}}}\right)\right]\delta_{\mathrm{v,v'}} \quad (7)$$

$$\langle m'_{\sin}, v'|H|m_{\sin}, v\rangle = \left[\left\{\left(m_{\sin}^2 B + \frac{V_6}{2}\right) + \frac{1}{200\pi c}\left(v+\frac{1}{2}\right)\left(\frac{k}{\mu}\right)^{\frac{1}{2}}\right\}\delta_{\mathrm{m,m'}} + \frac{V_6}{2}\left(\delta_{\mathrm{m+m',6}} - \delta_{\mathrm{|m-m'|,6}}\right)\right]\delta_{\mathrm{v,v'}} \quad (8)$$

$$\langle m'_{\cos}, v'|H|m_{\sin}, v\rangle = \frac{K_{\theta q}\alpha}{400hc}(v+v'+1)^{\frac{1}{2}}(\delta_{\mathrm{m+m',3}} + \delta_{\mathrm{m-m',3}} - \delta_{\mathrm{m-m',-3}})\delta_{\mathrm{|v-v'|,1}} \quad (9)$$

$$\alpha = \left(\frac{\hbar^2}{\mu k}\right)^{\frac{1}{4}} \quad (10)$$

where $m_{\sin}$ and $m_{\cos}$ are the quantum numbers for sine and cosine functions, while v is the quantum number for the harmonic oscillator. We determined four parameters B, V_6, k, $K_{\theta q}$ by the least squares method to reproduce the observed energy levels with the two-dimensional model using Eq. (5). It is reasonable to consider that the strongest band in each DF spectra as the levels in the S_0 state corresponding levels in S_1 state. But the observed band in $7e''$ level excited DF spectrum was so broad that we use the one observed in origin $(0a_1' + 1e'')$ excited DF spectrum. We used 50 functions for both even and odd symmetry ($m = 0$–50) for θ and 6 functions for q. These numbers were confirmed to be large enough to avoid a truncation problem in the range of lower eigenvalues targeted now. Since one of the three parameter (μ, k, $K_{\theta q}$) acts as dependent variable in these matrix elements, the reduced mass of the out-of-plane mode μ was fixed at 2.13 amu, which is the reduced mass of mode ν_2 in the S_0 state obtained by DFT calculation. The observed and calculated internal rotational levels in the S_1 and S_0 states are listed in Tables 2 and 3 together with the assignments. These assignments show the main character of the final states. The label for each state

Table 3
Observed and calculated internal rotational levels in S_0 of 9MA

$-\Delta\nu/cm^{-1}$			Assignment
Observed[a]	Calculated[b]	Observed[c] (Ref. [12])	
0	0	0[a]	$1e''$
0	1		$0a_1'$
77	71	79[a]	$5e''$
102	99	104[a]	$6a_1'$
118	125	123[c]	$7e''$
138	136		$2e'v$
157	156	158[c]	$3a_2''v$
182	186		$4e'v$

[a] Strongest band in each DF spectra (except $7e''$).
[b] Obtained with parameters $B = 3.3\ cm^{-1}$, $V_6 = 80\ cm^{-1}$, $k = 1.43\ Nm^{-1}$, $K_{\theta q} = -4.77 \times 10^{-11}$ N, and $\mu = 2.13$ amu.
[c] Observed bands in DF spectrum.

indicates the basis function that has the largest coefficients $C_{m,v}$ in Eq. (6). For example, $6a_1'$ is $\cos(6\theta)\exp\left(-\frac{q^2}{2\alpha^2}\right)$ and $3a_2''v$ is $\sin(3\theta)\frac{2q}{\alpha}\exp\left(-\frac{q^2}{2\alpha^2}\right)$. We obtained parameters $B = 2.1\ cm^{-1}$, $V_6 = 20\ cm^{-1}$, $k = 1.67\ Nm^{-1}$, and $K_{\theta q} = -5.16 \times 10^{-11}\ N$ for the S_1 state, and $B = 3.3\ cm^{-1}$, $V_6 = 80\ cm^{-1}$, $k = 1.43\ Nm^{-1}$, and $K_{\theta q} = -4.77 \times 10^{-11}$ N for the S_0 state, respectively. A typical value of internal rotational constant of methyl rotation is $B \approx 5\ cm^{-1}$, since the internal rotational constant is inversely proportional to reduced mass and that of methyl rotation is constant ($\mu \approx 1.0$–1.1 amu). The reduced mass of $\nu_{S0,1}$ is larger than that of pure methyl rotation when the methyl rotation is coupled with the out-of-plane bending motion. A small value of B results from the increase in the reduced mass due to the participation of the motions of other atoms. The parameter k is comparable with the force constant of ν_2. We calculated the Franck–Condon (FC) factors and compare to the experimental values in Fig. 8. The overlap integrals of two harmonic oscillator wave functions having different force constant were taken into account with notation given by Ansbacher [19]. The FC analysis reproduces the observed vibrational patterns in the FE and DF spectra. These results indicate that the internal rotation of the methyl group in 9MA should be described with multi-dimensional models.

4. Conclusions

The internal rotation of the methyl group in 9MA was investigated combining electronic spectroscopy in the gas phase with theoretical calculations. The observed low-frequency bands in the FE and DF spectra could not be reproduced with the one-dimensional model, because the methyl rotation of 9MA is not completely independent of the other motions of the atoms in the anthracene ring. Two-dimensional potential energy surfaces obtained by

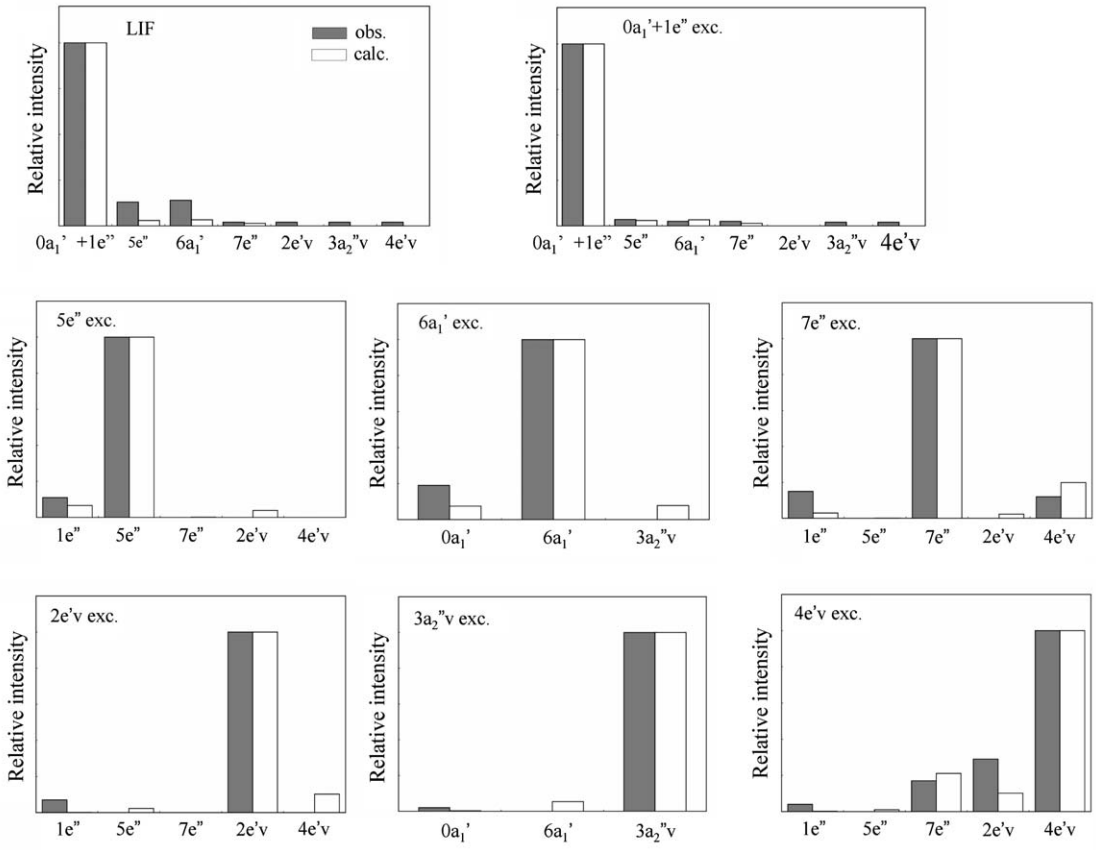

Fig. 8. Comparison of the observed and calculated intensities for the S_1-S_0 absorption and emission between the internal rotational levels of 9MA. The observed and calculated intensities are drawn with the shaded and white bars, respectively.

DFT calculations show the interaction between methyl rotation and the out-of-plane bending mode. Two-dimensional model Hamiltonian including the coupling term between the methyl rotation and the out-of-plane mode reproduce the observed vibrational patterns in the FE and DF spectra.

References

[1] K. Okuyama, N. Mikami, M. Ito, J. Phys. Chem. 89 (1985) 5617.
[2] Z.-Q. Zhao, C.S. Parmenter, D.B. Moss, A.J. Bradley, A.E.W. Knight, K.G. Owens, J. Chem. Phys. 96 (1992) 6362.
[3] R.A. Walker, E. Richard, K.-T. Lu, E.L. Sibert III, J.C. Weisshaar, J. Chem. Phys. 102 (1995) 8718.
[4] R.A. Walker, E.C. Richard, K.-T. Lu, J.C. Weisshaar, J. Phys. Chem. 99 (1995) 12422.
[5] H. Ikoma, K. Takazawa, Y. Emura, S. Ikeda, H. Abe, H. Hayashi, M. Fujii, J. Chem. Phys. 105 (1996) 10201.
[6] M. Nakagaki, E. Nishi, K. Sakota, K. Nishi, H. Nakano, H. Sekiya, Chem. Phys. 316 (2005) 178.
[7] H. Nakai, M. Kawai, Chem. Phys. Lett. 307 (1999) 272.
[8] H. Nakai, M. Kawai, J. Chem. Phys. 113 (2000) 2168.
[9] H. Nakai, Y. Kawamura, Chem. Phys. Lett. 318 (2000) 298.
[10] M. Kawai, H. Nakai, Chem. Phys. 273 (2001) 191.
[11] Y. Kawamura, H. Nakai, Chem. Phys. Lett. 368 (2003) 673.
[12] J.A. Syage, P.M. Felker, D.H. Semmes, F. Al Adel, A.H. Zewail, J. Chem. Phys. 82 (1985) 2896.
[13] W.R. Lambert, P.M. Felker, J.A. Syage, A.H. Zewail, J. Chem. Phys. 81 (1984) 2195.
[14] A. Mordziński, A. Leś, Y. Stepanenko, J. Rycombel, L. Adamowicz, J. Mol. Spectrosc. 233 (2005) 98.
[15] H. Mori, H. Kugisaki, Y. Inokuchi, N. Nishi, E. Miyoshi, K. Sakota, K. Ohashi, H. Sekiya, J. Phys. Chem. A 106 (2002) 4886.
[16] N. Tanaka, C. Okabe, K. Sakota, T. Fukaminato, T. Kawai, M. Irie, A. Goldberg, S. Nakamura, H. Sekiya, J. Mol. Struct. 616 (2002) 113.
[17] J.D. Lewis, T.B. Malloy Jr., T.H. Chao, J. Laane, J. Mol. Struct. 12 (1972) 427.
[18] M.J. Frisch, G.W. Trucks, H.B. Schlegel, G.E. Scuseria, M.A. Robb, J.R. Cheeseman, J.A. Montgomery Jr., T. Vreven, K.N. Kudin, J.C. Burant, J.M. Millam, S.S. Iyengar, J. Tomasi, V. Barone, B. Mennucci, M. Cossi, G. Scalmani, N. Rega, G.A. Petersson, H. Nakatsuji, M. Hada, M. Ehara, K. Toyota, R. Fukuda, J. Hasegawa, M. Ishida, T. Nakajima, Y. Honda, O. Kitao, H. Nakai, M. Klene, X. Li, J.E. Knox, H.P. Hratchian, J.B. Cross, C. Adamo, J. Jaramillo, R. Gomperts, R.E. Stratmann, O. Yazyev, A.J. Austin, R. Cammi, C. Pomelli, J.W. Ochterski, P.Y. Ayala, K. Morokuma, G.A. Voth, P. Salvador, J.J. Dannenberg, V.G. Zakrzewski, S. Dapprich, A.D. Daniels, M.S. Strain, O. Farkas, D.K. Malick, A.D. Rabuck, K. Raghavachari, J.B. Foresman, J.V. Ortiz, Q. Cui, A.G. Baboul, S. Clifford, J. Cioslowski, B.B. Stefanov, G. Liu, A. Liashenko, P. Piskorz, I. Komaromi, R.L. Martin, D.J. Fox, T. Keith, M.A. Al-Laham, C.Y. Peng, A. Nanayakkara, M. Challacombe, P.M.W. Gill, B. Johnson, W. Chen, M.W. Wong, C. Gonzalez, J.A. Pople, GAUSSIAN 03, Revision A.2, Gaussian, Inc., Pittsburgh PA, 2003.
[19] F. Ansbacher, Z. Naturforschg. 14a (1959) 889.